Post Earthquake Embankment Failure, Seepage-Induced Liquefaction, and Void Ratio Redistribution

S. A. Bastani[1] and B. L. Kutter[2]

[1]Leighton Consulting, Inc., Irvine, California, USA
[2]University of California, Davis, California, USA

Abstract— **Effects of liquefaction-induced void redistribution have not been understood or applied in geotechnical engineering practice. Several earth dams, tailings dams, and slopes have failed or been severely damaged due to liquefaction during or after earthquakes. In a significant number of cases, liquefaction-induced failure of embankments occurred from seconds to hours after an earthquake. One mechanism for the delayed failure is the softening associated with redistribution of void ratio caused by gradients of pore water pressure in sloping ground with non-uniform permeability.**

A finite slope, made of Nevada Sand, was modeled in the large Geotechnical Centrifuge at UC Davis to evaluate post-earthquake deformations with an injection-induced liquefaction system. A constitutive model was developed to capture the behavior of sands with a minimum number of parameters to enable prediction of post-earthquake liquefaction and/or seepage-induced liquefaction. This constitutive model, based on Critical State concepts is obtained by adding five physically meaningful parameters to the conventional Mohr-Coulomb model. The constitutive model is shown to capture the essential features of sand behavior under monotonic drained and undrained triaxial loading and water injection in a simple shear test under a constant shear stress. Using this constitutive model, the failure mode of the centrifuge model due to seepage-induced liquefaction was studied utilizing the FLAC finite difference computer code.

A ¼ scale model of the embankment tested in the large centrifuge was also shaken in the small centrifuge at UC Davis. Void ratio redistribution phenomena were observed by the numerical model, indicating its influence on the deformation pattern of sands during and after injection and/or shaking. The results and comparison of the two centrifuge tests and the numerical model will be presented in this paper.

Keywords—**Liquefaction, Post Earthquake Failure, Void Ratio Redistribution**

INTRODUCTION

Examples of post-earthquake liquefaction-induced failures of embankments are reported by Dobry & Alvarez [1], Seed et al. [2], Okusa et al. [3], and Finn [4] based on the field case histories and by Malvick et al. [5] in a centrifuge test at UC Davis. In these cases, liquefaction reduced the material strength and failure occurred under static forces after the earthquake shaking. One mechanism for the delayed failure is the softening associated with redistribution of void ratio caused by gradients of pore water pressure in sloping ground with nonuniform permeability. This mechanism has been studied by Malvick et al. [5] and [6], Fiegel & Kutter [7], and Kokusho & Kojima [8].

For the present study, the post-earthquake liquefaction-induced failure of granular embankments was investigated by a static centrifuge test in which the water that might be produced during an earthquake due to densification of deep saturated soil was simulated by injecting a similar volume of water at the base of the model. This experiment was later modeled in ¼ scale in a smaller centrifuge which was shaken by a sinusoidal motion. The static centrifuge test was modeled by Fast Lagrangian Analysis of Continua (*FLAC*) computer code utilizing a new constitutive model as presented in this paper. For more details on the centrifuge and numerical models refer to Bastani [9].

CENTRIFUGE MODELS

The static (NAB4) and dynamic (NAB5) centrifuge test configurations are shown on Figs. 1 and 2, respectively. The centrifuge models consisted of a densified coarse sand (Monterey sand) layer beneath an embankment composed of a fine sand (Nevada sand) capped by a layer of low permeability silty clay (Yolo Loam, CL-ML). The coarse sand layer was utilized to spread the injected water in the first experiment.

Figs. 1 and 2 are drawn to scale so that other dimensions may be scaled from the figures based on the given dimensions. The slope angle for the models was 24.5 degrees. All dimensions are provided in the model scale. The average void ratio of the Nevada Sand was 0.74 and 0.73 corresponding to relative densities of 41 and 43 percent for NAB4 and NAB5, respectively. The sand was dilative at the confining pressures obtained in these experiments. The Yolo Loam had average undrained shear strength of about 8.9 kPa and a water content of 30 percent. The dynamic centrifuge model, NAB5, was ¼ the scale of the static one with a similar slope geometry; however, lengths of slope toe and crest were slightly different due to the centrifuge box dimensions. Since the small centrifuge radius (approx. 1 m) was much smaller than the large centrifuge radius (9 m), NAB5 surfaces were properly shaped/curved to match the level ground situation and to compensate for the radial acceleration field at the sides of the slope. The coarse sand was also densified and shaped to create a flat and rigid base for the Nevada Sand embankment. Base/input acceleration of NAB5 was designed to produce liquefaction at the top 25 mm of Nevada Sand after six cycles of shaking. The small centrifuge model, NAB5, was shaken with 10 cycles of sinusoidal ground motion with single amplitude of 7g and approximate duration of 0.25 seconds in the model scale.

The centrifuge models NAB4 and NAB5 were consolidated in several stages up to 10g and 40g, respectively.

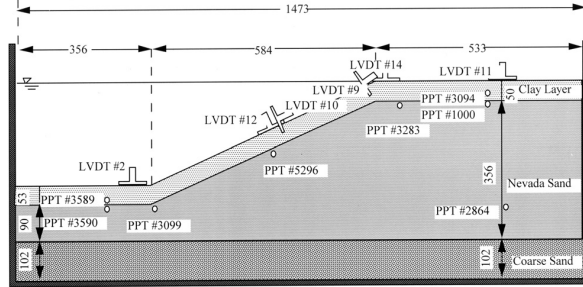All results presented in this paper are in the model scale.

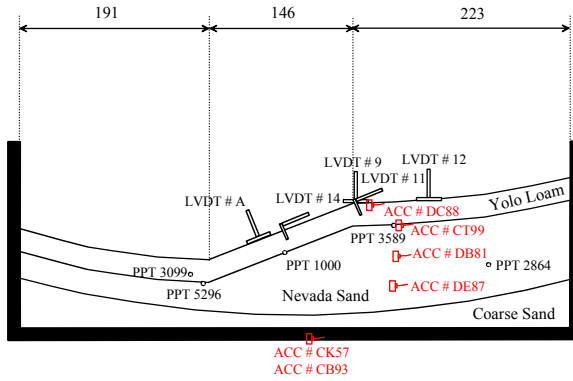Figure 1. Configuration of static test, NAB4, dimensions are in millimeters.

Figure 2. Configuration of dynamic test, NAB5, dimensions are in millimeters.

CONSTITUTIVE MODELS

A constitutive model was developed to simulate behavior of Nevada Sand in the *FLAC* program framework, and it was incorporated in the numerical modeling of the static centrifuge test. The purpose of this model was to predict the principal behavior of Nevada Sand with a minimum number of parameters that are physically defined and measurable.

The failure envelope for this constitutive model corresponds to the Mohr-Coulomb constitutive model (shear yield function) with tension cutoff (tensile yield function). The shear flow rule is non-associated and the tensile flow rule is associated. The shear potential function also corresponds to a non-associated flow rule. Details of Mohr-Coulomb model implementation are explained in the *FLAC* manual (Itasca [10]).

Several modifications are made to the Mohr-Coulomb model. The mobilized friction angle ($\phi_{mobilized} = \phi_{cs} + \phi_{dilation}$) is represented as a sum of the critical state friction angle (ϕ_{cs}) and the dilation angle ($\phi_{dilation}$) as suggested by Bolton [11]. ϕ_{cs} is considered constant, while the $\phi_{dilation}$ is assumed to be variable depending on the distance of the material state from the critical state line in e-log(p′) space, defined by the state parameter:

$$\psi = e - e_{cs} = e - (e_{cs})_a + \lambda \log \frac{p'}{p_a} \quad (1)$$

where e is the void ratio, $(e_{cs})_a$ is the critical state void ratio at one atmosphere, λ is the virgin compression slope, p' is the mean effective stress, and p_a is the atmospheric pressure.

Been and Jefferies [12] showed that the gradual change from dilative to contractive behavior could be quantified in terms of the state parameter ψ. The dilation angle ($\phi_{dilation}$) was modified based on the state parameter ψ and its changes according to equation [2].

$$\phi_{dilation} = (\phi_{dilation})_0 \cdot (1 - \frac{\Delta \psi}{\psi}) \quad (2)$$

where $\phi_{dilation}$ is the updated dilation angle, $(\phi_{dilation})_0$ is the initial dilation angle, ψ is the state parameter, and $\Delta \psi$ is the variation of the state parameter. The soil's bulk and shear moduli are also modified in the model. The bulk modulus (K) is evaluated utilizing equation [3].

$$K = \frac{p'(1 + e)}{\kappa} \quad (3)$$

where κ is the unloading slope and p' and e are defined as above. The shear modulus (G) was consequently determined based on the bulk modulus (K) and their elastic relationship in equation [4].

$$G = \frac{3(1 - 2\upsilon)K}{2(1 + \upsilon)} \quad (4)$$

where ν is effective stress Poisson's ratio. In summary, the constitutive model parameters are ϕ_{cs}, ν, κ, $(\phi_{dilation})_0$, λ, and $(e_{cs})_a$, and the material state is described by the void ratio.

The behavior of the constitutive model under selected load paths is presented in Fig. 3, which shows predicted paths for: conventional drained triaxial compression, conventional undrained triaxial compression, and a simple shear element subjected to a constant shear stress and water injection. Results are shown for deviator stress (q), mean effective stress (p'), volumetric strain (ε_v), void ratio (e), and shear strain (γ).

The constitutive model predicted the strain hardening behavior of the Nevada Sand during undrained shearing until cavitation occurred prior to reaching the critical state line. The predicted undrained path in Fig. 3 reasonably matched test results for the Nevada Sand with a relative density of 39.4% under the undrained condition in a triaxial test. Comparison of the calculated undrained stress paths with experimental data (not shown here) are presented by Bastani [9].

Under the drained condition, the model behavior exhibited elastic contraction up to the peak shear stress. Dilation started after the peak shear stress and continued up to the critical state condition.

Finally, the model behavior was studied under a constant shear stress and pore water pressure increase, modeling a simple shear test with pore fluid injection. The constitutive model slightly dilated prior to reaching the failure envelope; thereafter, the sample dilated with the increase of pore water pressure and the stress path approached the origin along the failure envelope in the *p′-q* space until it reached the critical state condition similar to the stress path suggested by Boulanger [13]. Similar stress path for sands were also observed in triaxial tests using similar procedures by Boulanger & Truman [14] and Vaid & Eliadorani [15].
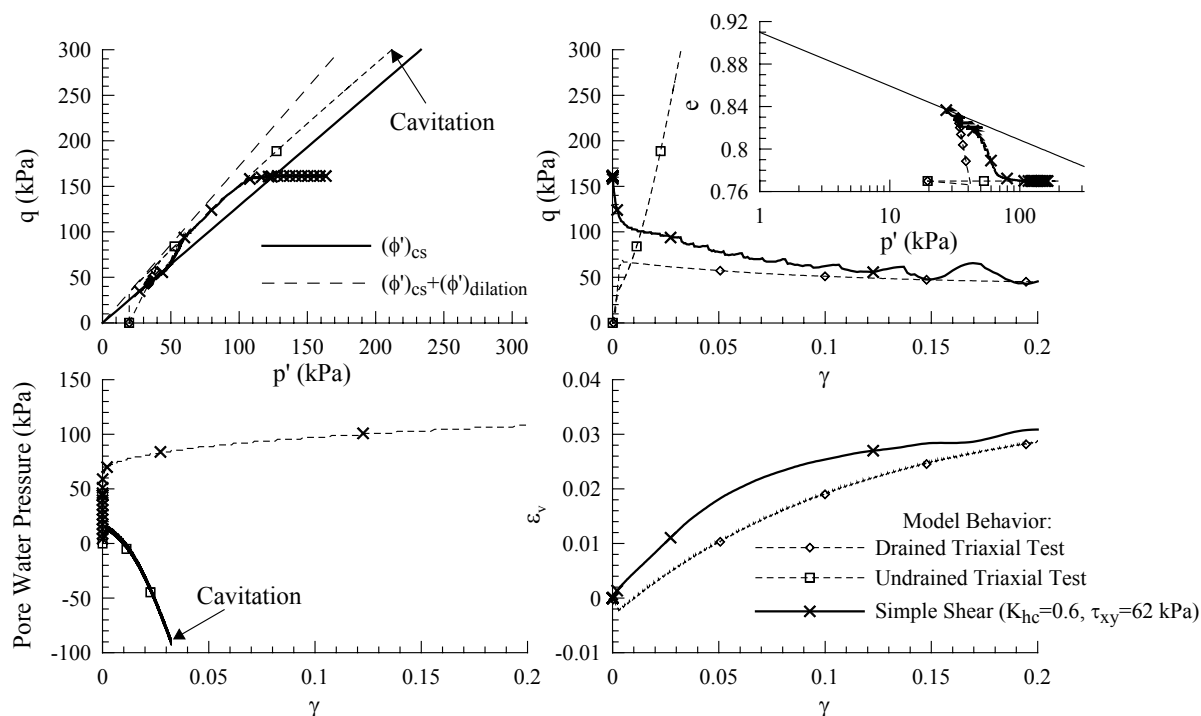
Figure 3. Behavior of the new constitutive model.

As expected, the water injection into the element led to an unstable condition and a dynamic collapse when the strength of the element dropped below the constant applied shear stress. The simulation was carried out in FLAC, so the stresses in the element could continue to be tracked, even during the unstable dynamic collapse. Some numerical oscillation is observed in the q-γ curves at shear strains greater than 0.12, but the softening behavior can still be clearly observed during the unstable collapse.

The parameters used for this calibration and later in the numerical modeling based on this constitutive model are provided in Table 1.

TABLE 1. MODEL PARAMETERS.

Parameters	Value
λ*	0.022
κ (=λ/5)	0.0044
ϕ_{cs} (degrees)	32
$(\phi_{dilation})_{max}$ (degrees)	10
ν	0.25
$(e_{cs})_a$*	0.809
Atmospheric pressure, p_a (kPa)	101.2

* Obtained from Archilleas et al. [16].

NUMERICAL MODEL OF NAB4

The *FLAC* run utilized the new constitutive model to predict the Nevada Sand behavior. This numerical model was bounded by its own limitations and those of the constitutive model; however, it was successfully used to observe both the general mechanism of localized increase in void ratio just beneath the less permeable silty clay layer and the failure mechanism; exact predictions were not expected. The *FLAC* run was performed in the large strain mode.

Fig. 4 shows the grid utilized in this model. The grid nodes and elements are identified in the subsequent fig-

ures with their column and row numbers (i,j). The column and row numbers increase from left to right and bottom to top, respectively.

Contours of mobilized volumetric strain, shear strain, and grid deformation patterns for this run are plotted in Fig. 5. This numerical model indicated the following behaviors:

1. Volumetric strains were concentrated along the interface of Nevada Sand and Yolo Loam layers;
2. Due to dilation, the mobilized friction angle was reduced to its critical state value along the Nevada Sand interface elements;
3. Shear strains were consequently concentrated at the slope interface within the Nevada Sand layer; and
4. Nevada Sand and Yolo Loam layers moved downward at the slope, which was translated to vertical uplift at the toe.

A significant, but smaller amount of dilation and shearing of deeper elements along the interface of Monterey Sand and Nevada Sand was also observed. It should also be noted that the development or lack of a deep failure mechanism was affected by the rate at which the water was injected relative to the permeability of the soils. For somewhat slower injection in the analysis, the deeper mechanism disappeared and only sliding along the bottom interface of the Yolo Loam was apparent. For much greater injection rates, a failure mechanism at the interface between the coarse Monterey Sand and the fine Nevada Sand was observed (Bastani [9]).

Stress/strain paths of several elements at the toe, along the slope, and at the slope crest are plotted in Fig. 6. In this figure, the shear strain is plotted on a logarithmic scale to allow visualization of behavior at small and large strains. Effective stresses of slope/leaning elements (20,14) and (25,18) reduced while oscillating around constant shear stresses up to the failure envelope. Shear stresses of elements (14,8) and (19,8) along the slope toe increased during the failure of leaning elements until

reaching the failure envelope. Stress paths moved toward the origin after reaching the failure envelope and strain softening was observed. The stress path of toe elements moved away from the origin along the failure envelope in p'-q space without any additional shearing when the injection was halted; however, the slope and crest elements slightly dilated and showed additional shear strains after termination of injection. In general, the elements at the toe and along the slope showed higher shear strengths prior to the diving of their stress paths toward the origin due to the ability of the modified constitutive model to withstand a mobilized friction angle greater than the critical state friction angle during dilation. The volumetric strain rate of elements was drastically increased when the elements yielded either in shear or volume as shown by element (20,14). The volumetric strains were stabilized wherever the injection did not cause the strength to fall below the applied shear stress.

Predicted pore water pressures and deformations for the static centrifuge test, NAB4, are compared with the experimental results in Figs. 7 & 8. Pore water pressures were over-predicted for PPT #2864 at depth and PPTs #3590 and #3099 at the slope toe. The stress state of element (20,14) was very close to critical state prior to injection, therefore, high pore water pressure was not numerically developed prior to reaching   failure at this element. Pore pressure predictions were very good at the crest of the embankment. In general deformation predictions were very good.

The numerical model successfully predicted the dilatancy to cause a very loose layer of sand below the less permeable layer of Yolo Loam. The calculated volumetric strains of the dilated sand indicate a negligible residual strength after dilation.

COMPARISON OF STATIC AND DYNAMIC TESTS

 Centrifuge test NAB5 modeled the NAB4 in a ¼ scale. NAB5 was shaken with 10 cycles of acceleration with single amplitude of 7g as shown on Fig. 9. The acceleration time histories showed that at the slope crest the motions were damped after four cycles (Fig. 9).
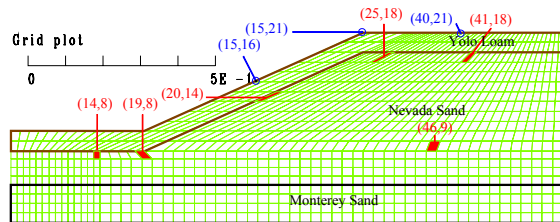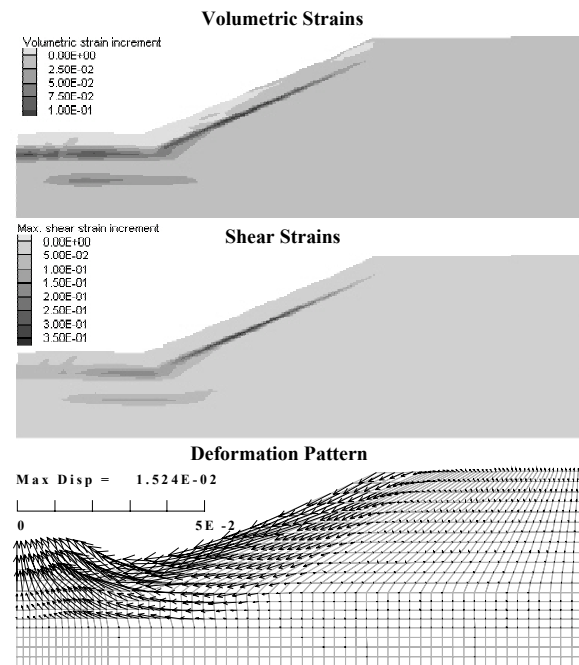

Figure 4. *FLAC* mesh.

Figure 5. Volumetric and shear strains and deformation patterns after 5 seconds of seepage in *FLAC* model.
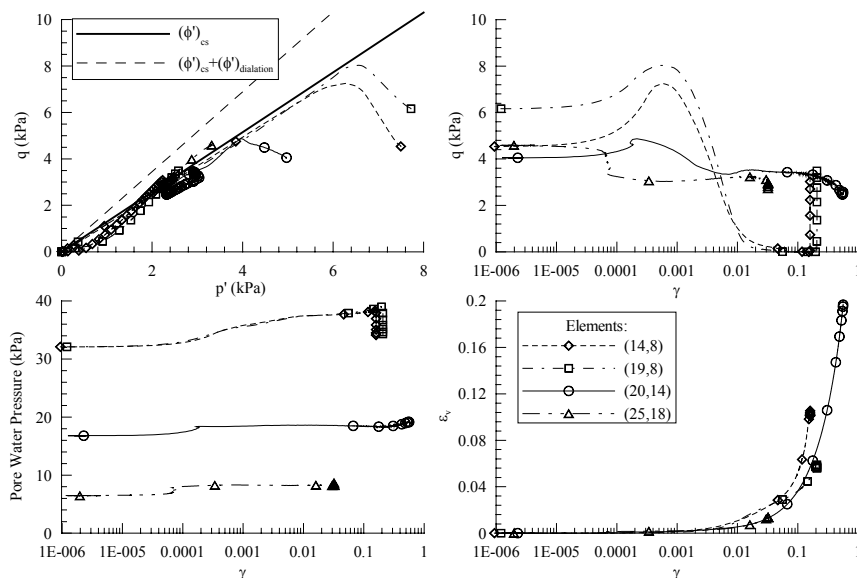

Figure 6. Stress and strain paths and behavior of elements in *FLAC* model.

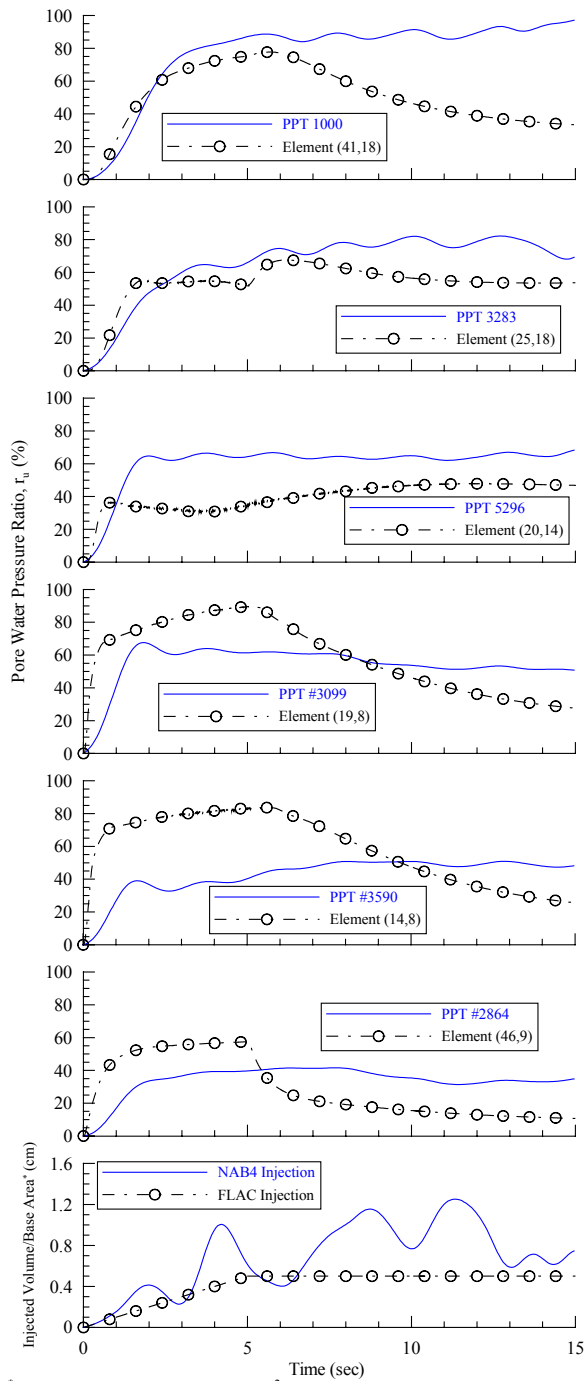* Centrifuge base area = 8,981 cm²

Figure 7. Comparison of pore water pressure time histories.

Acceleration spikes due to de-liquefaction of sand, as explained in Kutter and Wilson [17], were also observed at the slope crest (ACC #DC88 and #CT99) and at the middle of sand (ACC #DB81) layer.

To compare NAB4 and NAB5 pore water pressure and deformation time histories, time in NAB4 was normalized by the injection time and time for NAB5 was normalized by the shaking duration in Figs. 10 and 11. The pore water pressure ratio for the transducer #1000 oscillated greatly in the NAB5 result, which was possibly due to the inertia of water in front of the embankment that may have caused a change of total stress during the shaking and cyclic dilation of the Nevada Sand. These oscilla-

tions were not observed in NAB4 since the model was not shaken.

Pore pressure transducer #5296 of NAB5 also shows large oscillations. Pore pressure transducer #3589 shows much less oscillation relative to the other transducers. Lack of oscillations in the PPT #3589 in NAB5, and the fact that it lags behind the result of NAB4 measurement could be due to partially clogged porous stone for PPT #3589 in NAB5.

The NAB4 pore water pressure trend matches the average trend of pore water pressure generation in NAB5 along the slope. The only exception was that the pore water pressure ratio at the deeper part of the embankment was much smaller during injection than during shaking as shown by PPT #2864 in Fig. 10 for NAB4 and NAB5, respectively. After shaking stops the pore pressure ratios in the static and dynamic experiments are very similar everywhere.

The consistency in pore pressure results between the static and dynamic experiment is consistent with the idea that the pore pressures have reached a limiting condition corresponding to the intersection of the applied shear stress and the phase transformation line. This is similar to the limiting r_u concept described by Malvick et al. [6] and Bastani [9].
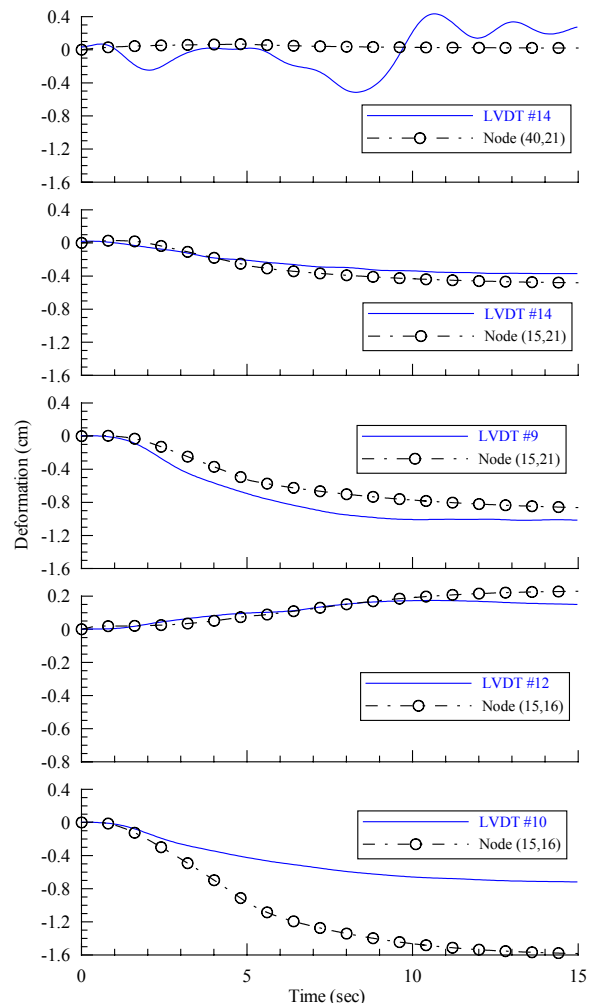

Figure 8. Comparison of deformation time histories for NAB4.

After stopping the centrifuge, the surface profiles were measured, cracks were mapped, and the sample was dissected. From these observations it was clear that failure/shearing occurred primarily in the partially liquefied sand layer rather than the overlaying silty clay layer. Comparison of the measured deformations in Fig. 11 shows that NAB5 deformations were equal to three times greater than the deformations in NAB4 in the model scale; NAB5 was 1/4 scale of NAB4. Taking this into account deformations in NAB5 were about four to 12 times greater at prototype scale.

The local drainage inside the model was calculated in the FLAC model of experiment NAB4. Volumetric strain rate of several elements along the slope are plotted versus their normalized time in Fig. 12 for purposes of comparison. Since Nevada Sand at 40% relative is dilative during monotonic loading, the assumption of partially drained failure of elements at the interface of Yolo Loam and Nevada Sand is logical. Fig. 12 shows that the predicted volumetric strain rates were reduced at the end of the injection and shaking events, at the same time the rate of predicted deformations were also reduced at the end of injection/shaking (See Figs. 8 and 10). After injection and shaking the deformations continued with lower rates in the analysis, which were directly correlated to the volumetric strain rates of the interface elements.

The deformation rates after injection and shaking were lower in the experiment compared to analysis. This difference may be due to crack formation through the less permeable top layer which allowed water to escape without accumulating at the interface. Cracking was not accounted for by the numerical model.

Existence of these cracks directed the internal pore fluid flow to the outside and prevented further dilation of interface elements. Predicted volumetric strains quickly increased at the elements that yielded either in volume or shear, as shown by Element No. (20,14) in Fig. 12. The difference in post-injection deformation could also be explained by imperfections in the constitutive model.

Shaking or injection causes increase of pore water pressure which makes the stress state of elements move toward the failure envelope. After reaching the failure envelope, elements continue to shear under dynamic plus static shear stresses or static stresses as long as the pore water flow required for dilation of the material is available due to the hydraulic gradients inside the system.

If the soil remains in a dilatant state with constant applied shear stress at the end of shaking, shearing will cease when injection/dilation stops, which will be due to change of the mode of failure from drained water injection mode to undrained shear mode. Since the material is dilative, in undrained circumstances, additional shear strains will be obtained only if the applied shear stresses increase.

In tests NAB4 and NAB5, static shear stresses are less than the undrained strength after minor deformations and therefore displacements cease when volumetric dilations stop.
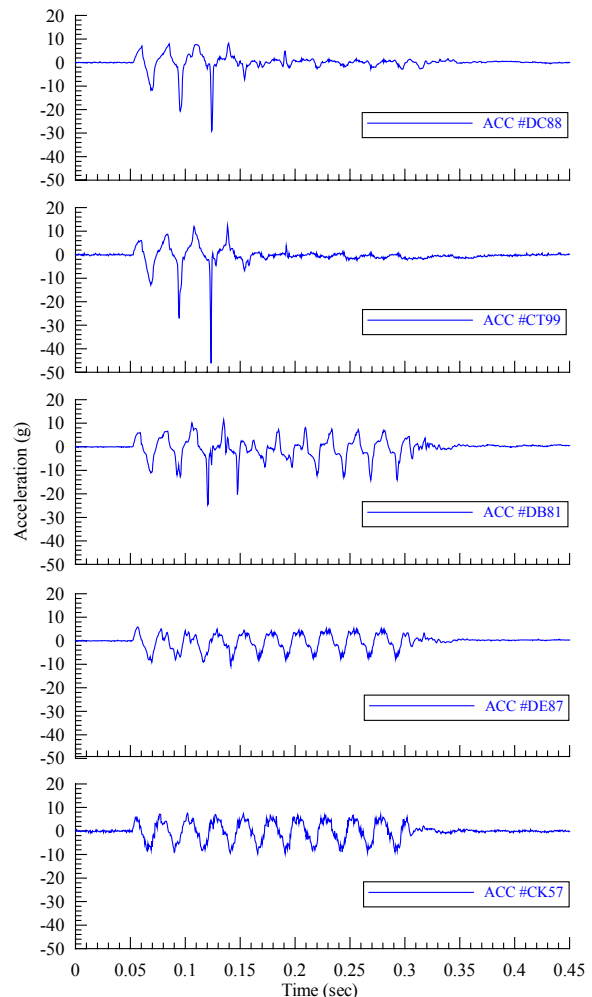

Figure 9. Comparison of acceleration time histories.

CONCLUSIONS

A centrifuge test was performed using a shaker to induce liquefaction in a slope covered by a less permeable layer in a dynamic experiment. The pore water produced by vibration of liquefiable soil was also simulated by the water injection system in a centrifuge experiment without shaking.

If sloping ground is made of contractive soil, a sudden increase of pore water pressures or dynamic shaking will push the stress state of the soil element towards the failure envelope and may trigger the undrained flow failure mechanism of the soil elements. However, generation of shear strains/deformations for the dilative soils will be restricted by the availability of water for dilation. Less permeable layers of soil retain pore water that may be made available on a delayed time scale to dilating soil on a potential failure mechanism.
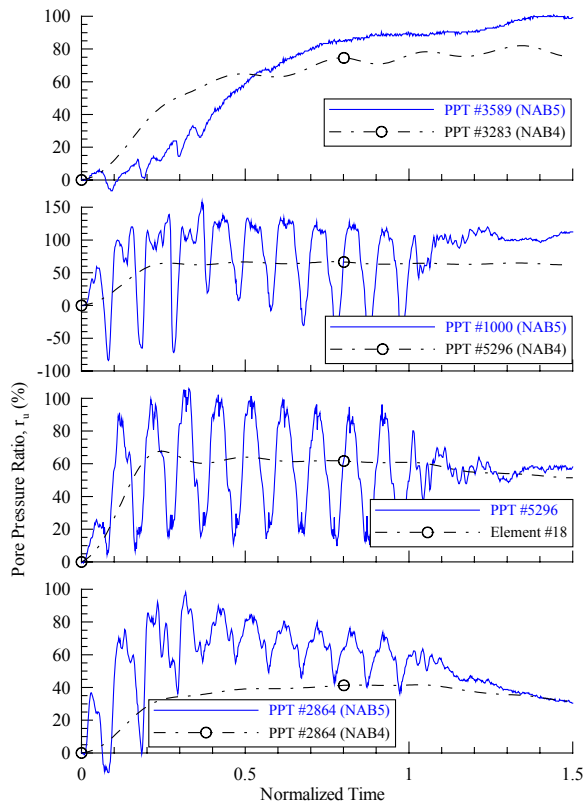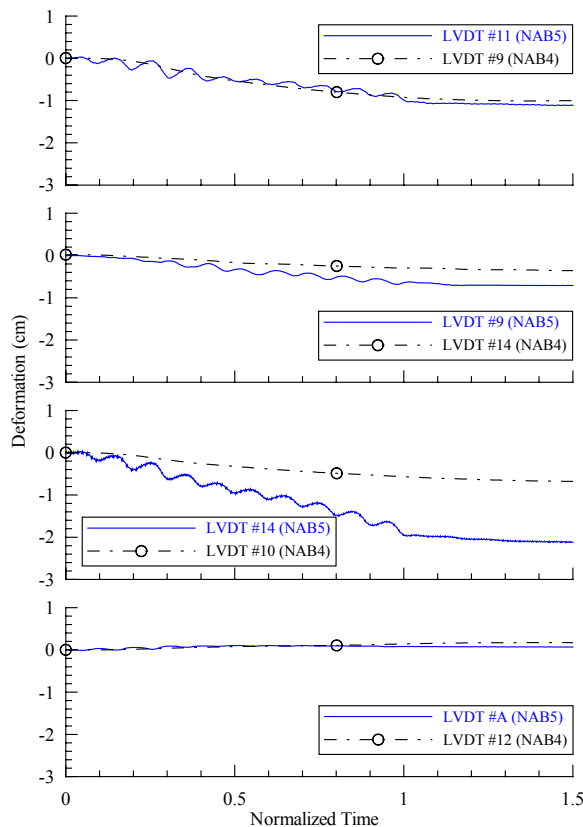
Figure 10. Pore water pressure comparison.

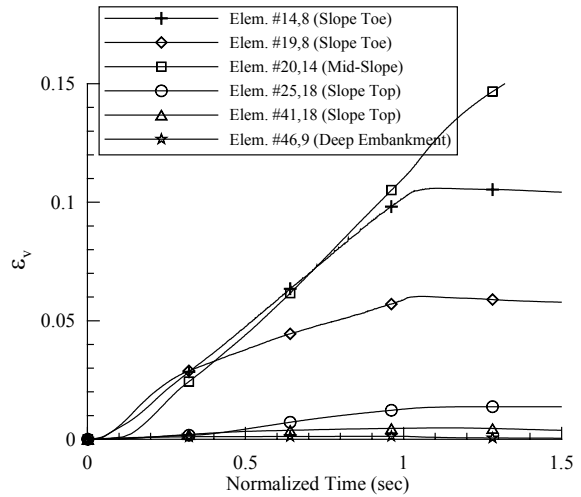Figure 11. Comparison of deformations.

Figure 12. Volumetric strains within NAB4.

A modified Mohr-Coulomb constitutive model was developed based upon critical state theory in conjunction with a new expression for dilatancy that depends on the state parameter (the distance between the state and the critical state). The constitutive model was shown to enable calculation of strain softening paths, and dilation due to water injection.

The constitutive model was implemented in FLAC and used to analyze results of centrifuge model tests of layered sloping ground subject to pore fluid injection. The injection was intended to simulate the upward flow of water that might be generated by densification of deep soil deposits during earthquake shaking.

From one perspective, embankments made of dilative material may be considered to be safe, because the undrained strength is greater than the driving stress as explained by Poulos et al. [18]. The centrifuge tests and the FLAC analyses presented here, however, clearly demonstrate the possibility that layers that impede drainage may cause a significant localized zone of softened material that should be considered as a possibility in seismic design. To determine induced deformations due to local drainage of a system, a material model that captures this process should be incorporated in the numerical model. The mode of failure and local drainage of the centrifuge test presented here was successfully predicted utilizing the modified Mohr-Coulomb constitutive model in conjunction with FLAC numerical framework.

An apparent difference between dynamic- versus injection-induced liquefaction is the lack of seismic inertia forces and dynamic deformations in the latter condition. A similar concept is also applicable to the during- and post-earthquake liquefaction-induced failures. As observed in NAB4 and NAB5, the deformation/failure during shaking occurred faster and with a larger magnitude compared to the injection-induced one. This behavior was also observed in the violent failure of the Mochikoshi Tailings dike No. 1 during 1978 Izu-Ohshima-Kinkai earthquake (main shock) with a magnitude of 7.0 that was reported to be quick/violent, leaving splash marks as high as 30 m on leaves and branches of forest trees along its path through a valley with a bed slope of 15°, at high speed like a bluish white river for about 7-8 km versus the less violent post-earthquake failure of dike No. 2 where tailings ad-

vanced slowly into another valley of about 10° slope for a distance of 150-240 m, as explained by Okusa et al. [3].

In the NAB4 and NAB5 centrifuge tests the deformations ceased after injection and shaking, respectively. The numerical model showed small additional deformations due to the additional void ratio redistribution within the model after completion of the injection and shaking. Longer drainage paths and/or lower permeability would be expected to cause the redistribution to continue for a longer time after injection and shaking. Both experimental results and the numerical model indicate that deformations increase with a smooth relationship to the injected volume of fluid; larger deformation will be expected with a larger injection volume. In order to make a prediction of rate and magnitude of injection-induced/post earthquake deformations in field conditions, it is necessary to predict the redistribution of pore water flow in the ground, and to have a constitutive relationship that reasonably predicts shear strains caused by pore water redistribution/injection. We have presented a constitutive model that captures essential features of the static injection problem. An unsolved segment of this problem, making it difficult to apply in practice, is the need to have an accurate model of the heterogeneous geometry of the permeability of all deposits and liquefiable deposits in field situations.

REFERENCES

[1] Dobry, R. & Alvarez, L. 1967, "Seismic Failure of Chilean Tailing Dams," *Journal of Soil Mechanics and Foundations Division*, Proceeding of the American Society of Civil Engineers 93 (SM6): 237-260.

[2] Seed, H.B., Lee, K.L., Idriss, I.M., & Makdisi, F.I. 1975, "The Slides in the San Fernando Dams during the Earthquake of February 9, 1971," *Journal of the Geotechnical Engineering Division*, ASCE 101(GT7), pp. 651.

[3] Okusa, S., Anma, S., & Maikuma, H. 1978, "Liquefaction of Mine Tailing in the 1978 Izu-Ohshima-Kihkai Earthquake, Central Japan," *Engineering Geology* Vol. 16, pp. 195-224, Elsevier Scientific Publishing Co.

[4] Finn, W. D. 1980, "Seismic Response of Tailing Dams," *Presented at Seminar on Design and Construction of Tailing Dams,* Colorado School of Mines, Denver, Colorado, pp. 76-97.

[5] Malvick, E.J., Kutter, B.L., & Boulanger, R.W. 2004, "Post-Shaking Failure of Sand Slope in Centrifuge Test," *Proceedings of the 11th International Conference on Soil Dynamics & Earthquake Engineering & 3rd International Conference on Earthquake Geotechnical Engineering Conference,* Berkeley, CA, in press.

[6] Malvick, E.J., Kulasingam, R., Boulanger, R.W., & Kutter, B.L. 2003, "Analysis of a Void Ratio Redistribution Mechanism in Liquefied Soil," *Proceedings of 12th Pan-American Conference on Soil Mechanics & Geotechnical Eng*ineering, Cambridge, MA. pp. 955-961.

[7] G. L. Fiegel & B. L. Kutter. 1994, "Liquefaction-induced lateral spreading of mildly sloping ground." Journal of Geotechnical Engineering., ASCE, 120(12), pp 2236-2243.

[8] Kokusho, T. & Kojima, T. 2002, "Mechanism for Postliquefaction Water Film Generation in Layered Sand," *Journal of Geotechnical Engineering*, ASCE 128(2): 129-137.

[9] Bastani, S.A. 2003, "Evaluation of Deformations of Earth Structures due to Earthquakes," *Dissertation presented to University of California, at Davis*, in partial fulfillment of the requirements for the degree of Doctor of Philosophy.

[10] Itasca Consulting Group, Inc. 2001, "*FLAC* - Fast Lagrangian Analysis of Continua, Version 4.0 User's Manual," Minneapolis, MN: Itasca.

[11] Bolton, M. 1991, "A Guide to Soil Mechanics," *Published by M D & K Bolton, Printed by Chung Hwa Book Company*, pp. 63-92.

[12] Been, K. & Jefferies, M.G. 1985, "A State Parameter for Sands," *Geotechnique* 35(2), pp. 99-112.

[13] Boulanger, R.W. 1990, "Liquefaction Behavior of Saturated Cohesionless Soils Subjected to Uni-Directional and Bi-Directional Static and Cyclic Simple Shear Stresses," *Dissertation presented to University of California, at Berkeley*, in partial fulfillment of the requirements for the degree of Doctor of Philosophy.

[14] Boulanger, R.W., & Truman, P. 1995, "Void Redistribution in Sand Under Post-Earthquake Loading," *Canadian Geotechnical Journal*, vol. 33, pp. 829-834.

[15] Vaid, Y. P. & Eliadorani, A. 1998, "Instability and Liquefaction of Granular Soils under Underained and Partially Drained States," *Canadian Geotechnical Journal*, vol. 35, pp. 1053-1062.

[16] Archilleas, G.P., Bouckovalas, G.D., & Dafalias, Y.F. 2001, "Plasticity Model for Sand Under Small and Large Cyclic Strains," *Journal of Geotechnical Engineering*, ASCE 127(11), pp. 973-983.

[17] Kutter, B. L. , & Wilson, D. W. (1999) "De-Liquefaction Shock Waves," *Proceedings of the Seventh U.S.-Japan Workshop on Earthquake Resistant Design of Lifetime Facilities and Countermeasures Against Soil Liquefaction*, Technical Report MCEER-99-0019, pp. 295-310.

[18] Poulos, S.J., Castro, G., & France, J.W. 1985, "Liquefaction Evaluation Procedure," *Journal of the Geotechnical Engineering Division*, ASCE 111(6), pp. 772-792.